Noname manuscript No.
(will be inserted by the editor)

Impulsive dispersion of a granular layer by a weak blast wave

V. Rodriguez · R. Saurel · G. Jourdan · L. Houas

Received: date / Accepted: date

Abstract The dispersion of particles by blast or shock waves induces the formation of coherent structures taking the shape of particle jets. In the present study, a blast wave, issued of an opened shock tube, is generated at the center of a granular ring initially confined in a Hele-Shaw cell. With the present experimental set-up, solid particle jet formation is clearly obtained and observed in a quasi-two-dimensional configuration. In all instances, the jets are initially generated inside the particle ring and thereafter expelled outward. Furthermore, thanks to the two-dimensional experimental configuration, a general study of the main parameters involved in these types of flows is performed. Among them, the particle diameter, the density of the particles, the initial size of the ring, the shape of the over pressure generated and the surface friction of the Hele-Shaw cell are investigated. Empirical relationships are deduced from experimental results.

Keywords explosive event simulation · blast waves · granular medium

1 Introduction

Explosions in granular and dusty media induce dispersion effects with unstable interface [1]. Example for such phenomenon in nature occurs in volcanic eruptions [2]. It is also observed during explosions of supernovas or when a solid projectile impacts a granular medium [3]. This kind of phenomenon also appears in accidental dispersion such as, for example, explosions of grain silos or in industrial plants using powders and even liquids. The granular medium does

E-mail: vincent.rodriguez@univ-amu.fr
V. Rodriguez · G. Jourdan and L. Houas
Aix-Marseille Université, IUSTI, UMR CNRS 7343, Marseille, France.

R. Saurel
Aix-Marseille Université, CNRS, Centrale Marseille, M2P2 UMR 7340, 38 rue J. Curie, 13541 Marseille, France.

not expand homogeneously. Actually, jet-like patterns are formed all around the particle front. Although the behaviour is very common, the governing mechanism of this instability is, as yet, not well understood. Such events can be described as shown in Fig.1. At t=0, a cluster of solid particles surrounds a gas pocket (Fig.1(a)). When the spherical membrane is ruptured, a pressure wave is created and propagates in the granular medium. The particle dispersion process begins at this moment. Preferred directions in particle density and velocity appear all around the expanding front. Consequently, particle jets appear and grow with time (Fig.1(b)). This phenomenon is considered in the present paper. Most of the previous experimental observations have been carried out so far in three-dimensional quasi-spherical configurations using explosives surrounded by granular layers [4–8]. Certain trends have been pointed

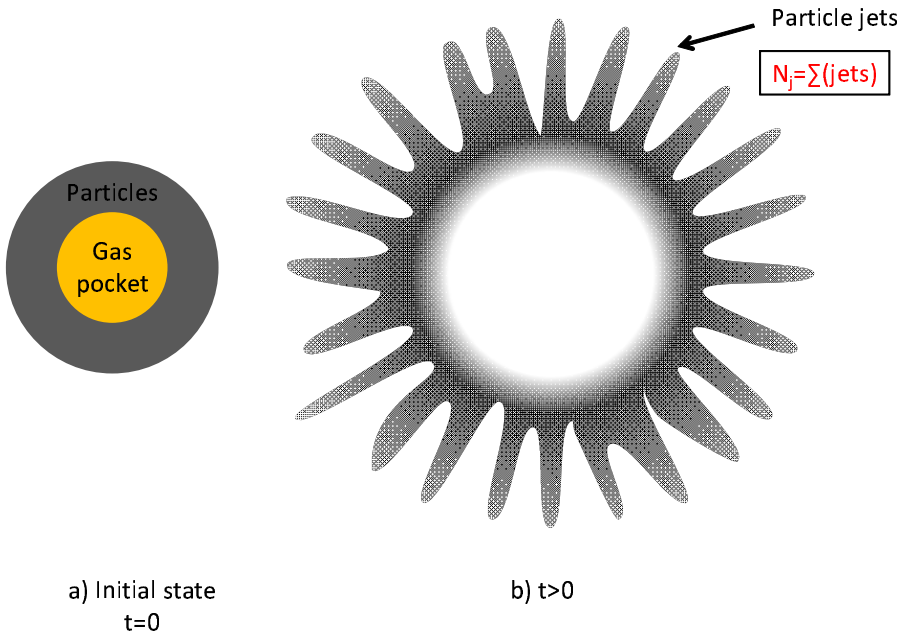

Fig. 1 Schematic description of solid-particle jet formation under gas expansion.

out in these studies. First, the dispersion of the particle layer depends on the ratio between the weight of the particles and that of the explosive [4]. Also, there exists a minimum layer velocity for the observation of jets [8]. Below this velocity, particle jets are absent. Furthermore, the formation of jets seems to start very early in the process. However, the three-dimensional nature of such configurations increases the difficulty in analysing experimental results. A more focused study was recently carried out by Frost *et al.* [9]. In that work, dispersion was performed by means of explosives in cylindrical configuration to reduce three-dimensional effects. The solid particles were initially saturated with liquid. The results showed that wet particles produce more jets than dry

beds ones, similar behaviour appearing with liquids. The dispersion of pure liquid produces many more jets than dry granular beds as well as liquid-grain mixtures [10]. A very recent paper by Zhang *et al.* [11] demonstrated experimentally the dual hierarchical jet structure consisting of primary particle jets overlapped by fine particle jets on the primary surface. In that paper, as observed in the very different pressure range of weak blast waves [12,13], the primary jet structure originates in the interior boundary between the explosive and the payload, while the fine jet instabilities are formed at the outside boundary between the payload and the air.

In addition to experimental studies, some numerical works have been conducted in parallel in order to support the experiments. Xu *et al.* [14] proposed a numerical study concerning solid particle dispersion at the mesoscopic scale in a cylindrical configuration. The results reveal that the mechanism of particle jetting can be induced by two parameters: the driver gas jets induced by the shock wave through the initial particle layer in the inner surface of the ring and the inelastic collisions between particles.

The aim of the present quasi-two-dimensional configuration set-up is to conduct reliable repetitive experiments using a ring of particles. This ring is accelerated in radial expansion, trapped in a Hele-Shaw cell. In Fig.2, the evolution of particle-jet formation in three-dimensional (3D) geometry (left picture), in cylindrical configuration (middle picture) and in the two-dimensional (2D) configuration developed in the present work (right picture). The first two experiments deal with explosively driven particle layers while the third one deals with blast waves in very different pressure range. The pressure gradient is very different but similar qualitative effects are observed in all experiments and configurations, giving interest in studies at low pressure gradients. Obviously, differences are present as grain's fragmentation and clustering are absent in low pressure gradient studies while they are present with explosive particle dispersal. In [12] focus was done on the effects of the incident shock

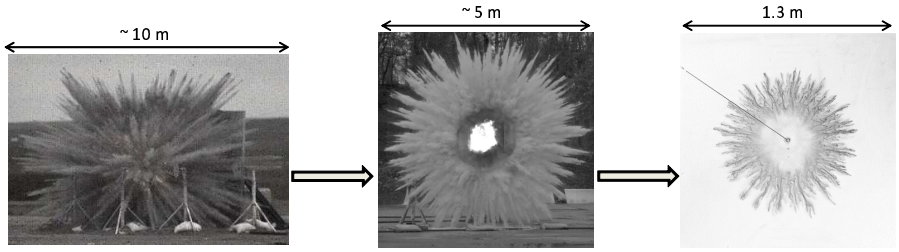

Fig. 2 History of studying particle-jet formation from 3D geometry to 2D in the recent past.

wave strength and effects of particle size. Then [13] was more focused on a study of small scale jets that appear at early times. From experimental re-

sults, empirical relationships for the considered phenomenon were suggested. In the present paper, a brief review of past and present results is done, to provide a comprehensive and clear picture. Additional experiments are done using new granular materials (PMMA and Talc), to study the influence of lighter and heavier materials compared to flour. In addition, wall friction is considered by adding a rough surface on the bottom plate. Finally, the first step of fractal analysis of the expanding ring is provided.

2 Experimental set-up

Experiments are carried out using a small conventional shock tube which produces moderate overpressure. The shock tube creates a blast wave at its exit which propagates radially into the Hele-Shaw cell. A schematic description of the experimental set-up is given in Fig.3. The shock tube (T32) has a inner

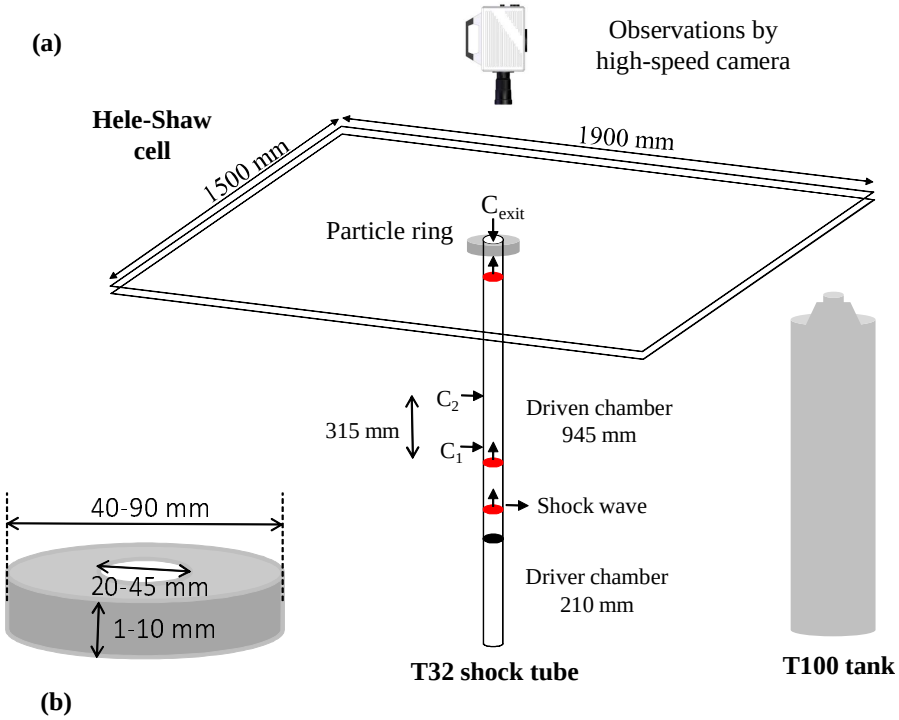

Fig. 3 General scheme of T32 shock tube, T100 pressurized tank and the 2D configuration with the Hele-Shaw cell (a). Schematic representation of the particle ring having variable dimensions (b).

diameter of 32 mm. It is fitted vertically beneath a Hele-Shaw cell, with a reduction of 20 mm, inside which the dispersion of particles takes place. The

incident shock wave is directed towards the center of the ring inducing the dispersion of the particle layer. The particle jet formation is recorded by a Photron Fastcam SA1 high-speed camera and the breaking mode of the granular layer subjected to an impulsive overpressure is studied from the recorded frames.

A small conventional vertical shock tube (T32) and a pressurized tank (T100) were alternatively vertically fitted beneath the Hele-Shaw cell. The first creates a blast wave at its exit, i.e. an impulsive pressure jump followed by a rapid pressure decrease. Its driver section is 210 mm long and its driven section is 945 mm long. A reduction of section of 20 mm is fixed to the T32 shock tube in order to correspond to the exit hole of the Hele-Shaw cell. Most of the experiments has been carried out with this tube. The use of the second (T100 tank) is interesting as it produces sustained shock waves. Recorded pressure histories at stations C_1, C_2 and C_{exit} (indicated in Fig.3) are given in Fig.4. The pressurized tank is 1150 mm long and 100 mm diameter with a reduction of 20 mm at its exit.

Moderate overpressures were used to observes in details particle dispersal. Several different materials were used; flour (finest corn flour), talc, PMMA and polystyrene spheres. Properties of these materials are given in Table 1. The particle size was measured using a particle size analyzer. These data are

Table 1 Particle properties where ρ_p and Φ_p are the material density and the particle diameter, respectively.

Particles	ρ_p (kg/m^3)	Φ_p (μm)
Flour	1530	14.5 ± 5
Polystyrene spheres	1050	10 ± 2
PMMA	1200	10 ± 2
Talc	2700	10.5 ± 2.5

in good agreement with those given in the literature for flour [16,17] and talc [18]. The initial particle ring diameters were 40 mm, 60 mm and 90 mm. The incident shock wave Mach number propagating inside the shock tube ranged from 1.1 to 1.45 and the corresponding overpressure peak varied from 0.7 to 4 bars. The granular material consisted of a ring of flour particles, polystyrene spheres, PMMA spheres and talc particles settled in the center of the cell and gently loaded between the plates using a mold (Fig. 5), around the outlet of the pressure generator and confined in a two-dimensional geometry allowing radial dispersion only. The internal and external surfaces of the particle ring are free of casings. Three pressure piezo-sensitive gauges were used in the present experiments. Two (C_1 and C_2) were located along the T32 conventional shock tube in order to determine the incident shock wave Mach number. The third (C_{exit}) recorded the pressure history at the center of the particle ring. To record the evolving flow pattern in the cell, a high speed digital camera Photron Fastcam SA1 was used with record frequency of 4,000 fps and a spacial resolution of 1,024×1,024 pixels.

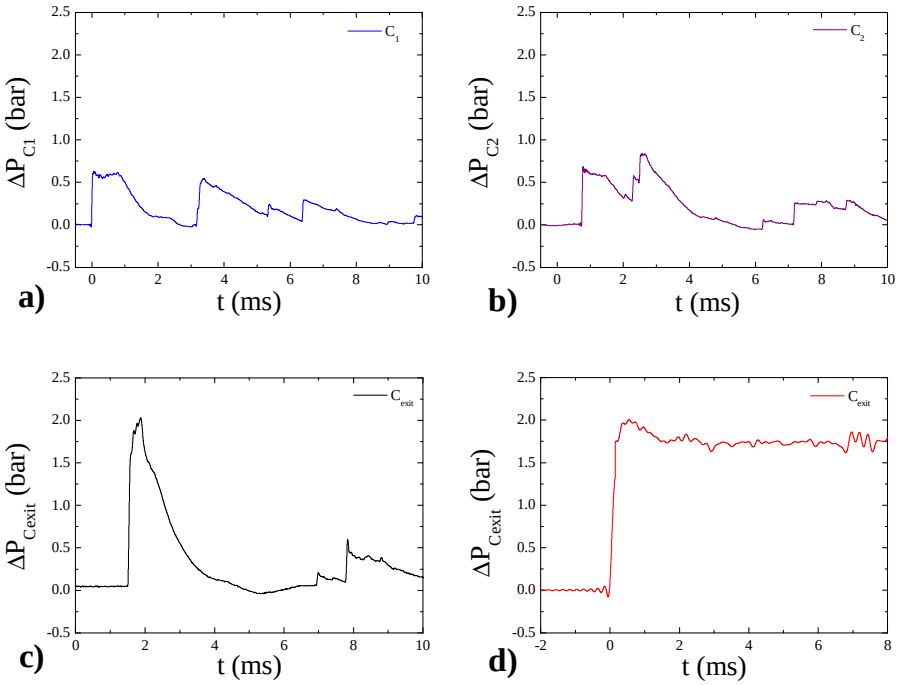

Fig. 4 Pressure history recorded by gauges C_1, C_2 and C_{exit} (a, b and c) when the T32 was used. (d) when the T100 was employed.

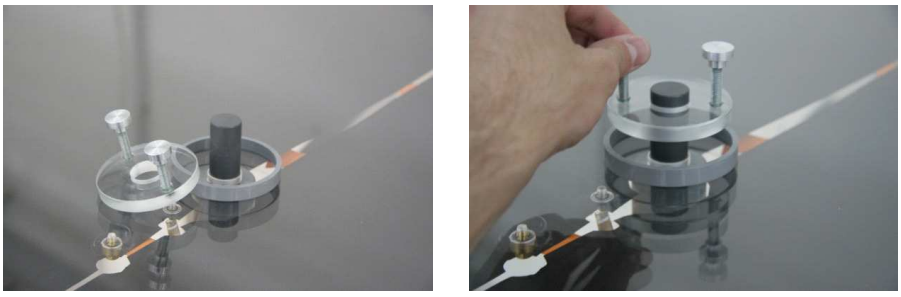

Fig. 5 Views of the tools used for producing the rings of particles: the mold, centering bar and piston.

3 Results

3.1 Sequence of events in the particle-jet-formation

Initially, the ring of particles surrounds the exit of the shock tube. Its initial diameter, R_0 is shown in the first frame of Fig.6. At t=0 the "blast wave" emerges from the shock tube exit and interacts with the particle ring. The particle ring compresses radially showing a perfect smooth external interface. The internal interface only moves radially; the external interface does not move. Thus, the

particle layer is compressed as shown in the second frame of Fig.6. However, all particles around the inner ring surface do not have the same velocity. Some particles are slower than others resulting in particle concentration fluctuation as shown in the third frame. Filaments appear regularly around the inner surface of the ring. These internal filaments are denoted J_i in Fig.6. Then, short wavelength perturbations appear on the outer surface of the ring as shown in the fourth frame. The wavelength of these small perturbations (along the ring outer surface) is smaller than those observed in the internal filaments J_i. These very thin external jets at short time are denoted by J_e^{st}. Afterwards, the outer shell of particles slows down whereas the filaments continue to move outwards (presumably due to lower drag) at a constant velocity, penetrating the outer particle shell and forming the appearance of jets. Consequently, the initial filaments cross the front and are expelled outside as shown in the fifth frame. Finally, these filaments become external jets at late times, denoted by J_e^{lt}. The number of external jets, decreases with time because of transverse motion. These latter jets are denoted by J_e^{vlt}. To summarize, there are four visible characteristic steps in the particle-jet formation: J_i, J_e^{st}, J_e^{lt} and J_e^{vlt}. In the present work the effects of shock wave intensity, pressure profile, particular ring geometry and surface friction have on the number of particle jets, only for J_i and J_e^{lt} (their number being the same) are studying. A complete study on the external jets at early time J_e^{st} was made previously [13]. Fig.7 allows more easily to understand how the jets are defined.

3.2 Influence of the pressure profile acting at the ring center on the particle jet selection

As mentioned earlier, when using the T32 shock tube, the pressure pulse in the granular medium ring, at the exit from the shock tube, is a blast wave (see Fig. 8(a)) and various wave reflections occur inside the tube, resulting in pressure oscillations. To better identify the origin of formation and selection of jets, a different experimental set-up is used; that produces a pressure pulse. In order to eliminate pressure oscillations and having a simpler pressure signal, the shock tube is replaced by a high pressure tank having 100 mm diameter. The corresponding volume is 50 times larger than that of the T32 shock tube. It is made of a driver section only, directly fitted beneath the Hele-Shaw cell. A schematic presentation of the T100 tank is shown in Fig. 3. This modification changes the time evolution of pressure as shown on top of Fig.8(b). The peak pressure level is the same in both cases (2 bars). Although these two pressure shapes are clearly different, we found that the jet formation in the solid particle dispersal, for both cases is very similar. The presence of the various perturbations i.e. J_i, J_e^{st}, J_e^{lt} are observed similarly. Moreover the number of particle jets is similar in both cases (Fig.8). As the dispersion of particles is more sustained for the tank configuration, as the positive pressure phase is longer, the main particle jets J_e^{lt} are more pronounced than in the T32 case. For the T32 case, the development of the thin perturbations J_e^{st} is

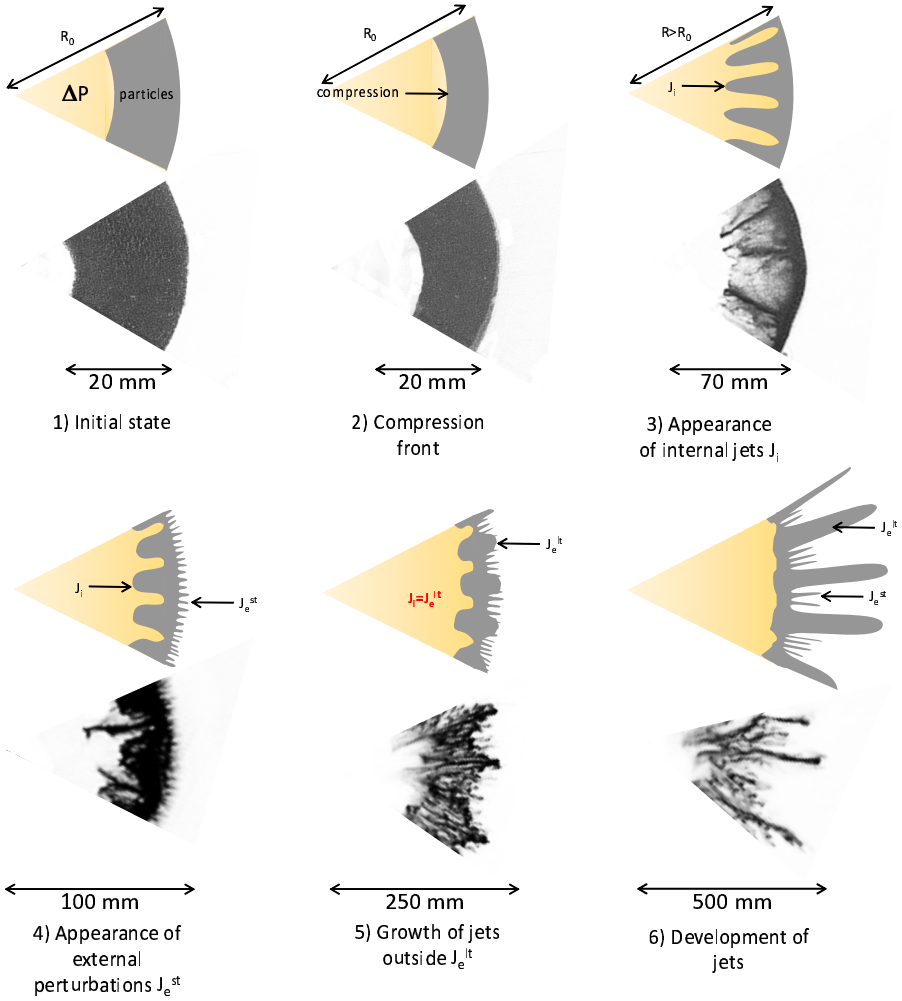

Fig. 6 Schematic representation of the different steps in the formation of particle jets with time and corresponding experimental visualization (below). R_0 is the initial radius of the ring, J_i represents the internal particle jets, J_e^{st} is the external front perturbations and J_e^{lt} corresponds to the external particle jets at late time. Pictures are not to scale. t=0 is the time when the shock wave reaches the inner surface of the ring.

more important and the main jets J_e^{lt} are less separable. We can conclude that the particle jet selection is not correlated to the shape of the pressure pulse, and in particular to the presence of pressure oscillations.

3.3 Influence of the initial pressure jump on the particle jet selection

Results from experiments, whose initial conditions are given in the table of Fig. 9, were conducted with the T32 shock tube. The aim is now to study

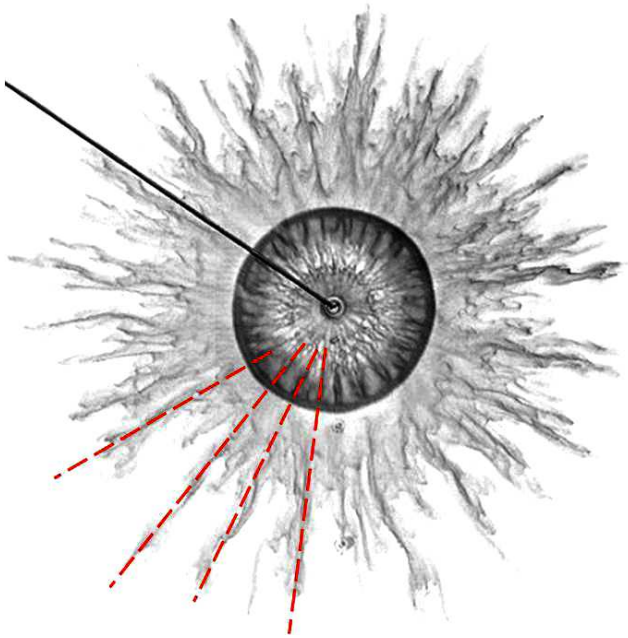

Fig. 7 Superposition of two frames taken at 6 ms and 57 ms after the initial acceleration of the particle bed showing the correlation between the internal particle filaments and the external jets. Dashed red lines show what is considered as a particle jet.

the influence of the initial pressure jump on particle jet number. First, the influence of the pressure jump was studied on a ring of flour particles. The initial pressure jump was varied from 0.5 bar to about 4.5 bars. The other parameters were kept fixed, namely the initial geometry of the particle ring. Fig. 9 presents results from four experiments with initial pressure jumps of 0.5 bar, 2 bars, 2.5 bars and 3.2 bars acting at the center of the ring, corresponding to initial shock wave Mach numbers of 1.07, 1.26, 1.32 and 1.39. As expected, we can observe that the dispersion is more intense for high shock wave Mach numbers. Moreover, the number of particle jets N_j, which corresponds to the J_e^{lt} jets, increases with the shock wave Mach number. All experimental results from this experiment are plotted in Fig.10, where N_j is the number of particle jets and $\Delta P_{C_{exit}}$ is the initial pressure jump acting at the center of the particle ring, respectively. These results clearly show that the number of particle jets increases with the initial pressure jump. Moreover, the shape of the curve presents a specific characteristic. On one hand, the curve has an asymptotic trend towards low pressures. This trend reveals that a minimum (about 15) number of jets could appear for a specific initial condition. On the other hand, the shape of the curve resembles a power law behavior when pressure increases. A fitted curve is superimposed based on the experimental findings and is the following: N_j=C$_0$+C$\Delta P_{C_{exit}}{}^k$ where C$_0$, C and k are constant parameters and $\Delta P_{C_{exit}}$ is the initial overpressure peak at the center of the particle ring.

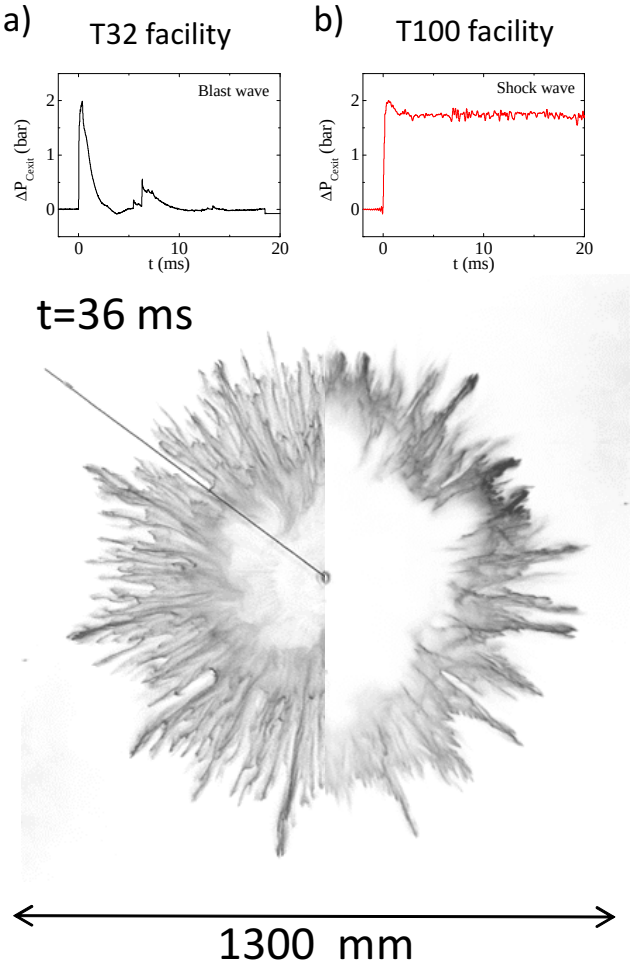

Fig. 8 Influence of the pressure profile imposed at the ring center for flour particles of 10 μm diameter. On the left, interaction with a blast wave created by the T32 facility; on the right, interaction with a sustainable shock wave created by the T100 facility. The pressure peak is the same in both cases (2 bars) but the pressure profile is not.

Based on the present experimental data, the correlation takes the following form: N_j=15+0.97$(\Delta P_{C_{exit}})^{2.1}$ for rings composed of flour particles.

3.4 Influence of the particle material on the jet selection

Several experiments have been done with different materials such as polystyrene spheres, PMMA spheres and talc particles. The average diameter of such particles is 10 μm as was for flour particles. Defining a non-dimensional parameter R: R=ρ_p/ρ_{ref}, where ρ_p is the density of the considered material and ρ_{ref} is

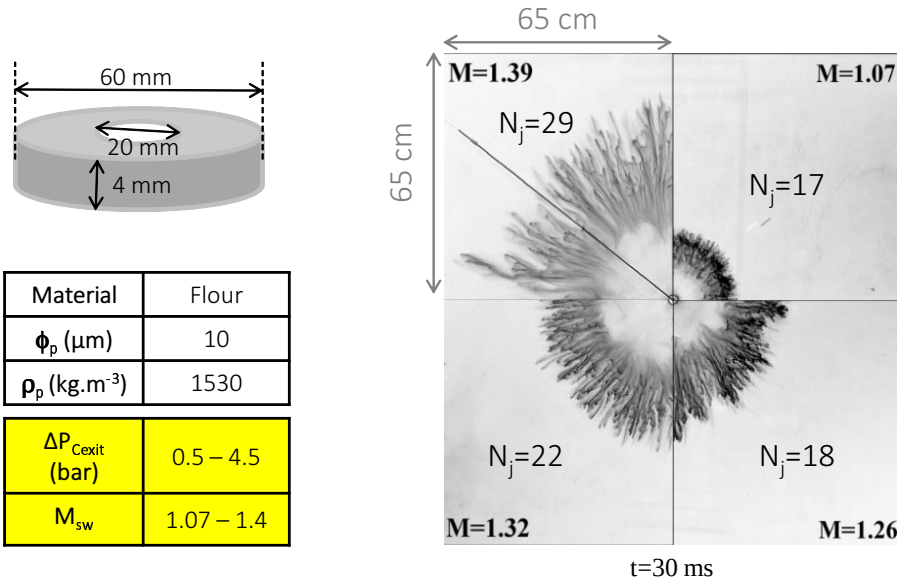

Material	Flour
ϕ_p (µm)	10
ρ_p (kg.m^{-3})	1530
ΔP_{Cexit} (bar)	0.5 – 4.5
M_{sw}	1.07 – 1.4

Fig. 9 Sequence of photos showing the influence of the initial shock wave strength on a flour particle ring. The changed conditions are given in the lower table.

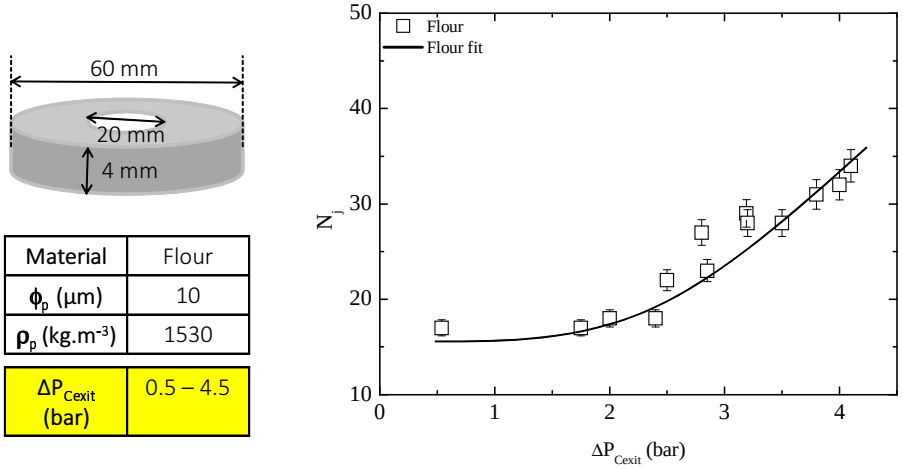

Material	Flour
ϕ_p (µm)	10
ρ_p (kg.m^{-3})	1530
ΔP_{Cexit} (bar)	0.5 – 4.5

Fig. 10 The number of jets N_j versus the initial pressure jump $\Delta P_{C_{exit}}$ at the center of the particle ring. The variable shock strength conditions are presented in the lower table. The empirical correlation expressing the evolution of number of jets as a function of pressure jump is: N_j=15+0.97$(\Delta P_{C_{exit}})^{2.1}$.

a reference density here the density of polystyrene, which is the lowest material density tested. In view of results presented in a previous work [12], the N_j axis is multiplied by R and the $\Delta P_{C_{exit}}$ axis is divided by R. Based on these results, an empirical relationship had been deduced. The correlation takes the following form: $N_j R$=22+3.35$(\Delta P_{C_{exit}}/R)^{2.1}$. Thus, the number of

jets changes depending on the factor R. According to this empirical relation, the higher R is, the lower the number of particle jets becomes. High R value corresponds to a high ratio of ρ_p/ρ_{ref}. Therefore, the higher the particle material density is, the smaller the number of particle jets becomes. Another way to represent the evolution of the number of jets is to plot $N_j \times$R versus the initial acceleration γ of the particle layer. This acceleration is deduced from experimentally reconstructed trajectories and averaged over the first three milliseconds. Previously, the evolution of jets was presented versus the quantity $\Delta P_{C_{exit}}/R$. The dimension of this quantity is similar to that of the acceleration γ. Moreover, this physical quantity is indirectly influenced by the initial pressure jump. An empirical relation has been deduced: $N_j R$=24+0.03$\gamma^{2.6}$ where γ represents the particle cloud acceleration.

Thereafter, experiments aimed at studying the influence of the particle diameter on number of jets are conducted. These experiments are done using polystyrene spheres with different diameters ranging from 10 μm to 250 μm. Results from [12] shows that the early time number of particle jets is independent on the particle diameter in agreement with previous observations done with liquids and powders [19].

3.5 Influence of the initial sizes of the particle ring on the particle jet selection

3.5.1 Influence of internal diameter of the particles ring

In the experiments presented in Fig.11, only the internal diameter of the ring is changed; the external diameter is fixed to 60 mm. Thus the radius of curvature related to the inner of the ring is changed. Photographs shown in Fig.11 indicate that this modification has not particular influence on the number of jets. The number N_j of particle jets in these three experiments is equal to 27±1. Consequently, the number of particle jets does not significantly change with changes made in the internal diameter of the particle ring.

3.5.2 Influence of external diameter of the particles ring

In the present study, the thickness of the particle layer remains constant. The experimental conditions are given in Fig.12. Moreover, in this figure, it is possible to observe that the number of jets increases with the external diameter of the ring. For the three investigated diameters 40 mm, 60 mm and 90 mm, the number of jets is equal to 13±1, 19±1 and 28±1, respectively. This behaviour seems to be proportional to the diameter. Thus, the quantity $N_j R$ is normalized by the initial external perimeter of the ring, πD_{ext}. The results, among others, are plotted at the end of this paper in Fig.17, which is a synthesis of the results of the present study. They show that N_jR$/\pi D_{ext}$ is invariant for a given shock pressure (or particle bed acceleration).

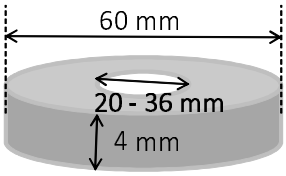

M_{sw}	1.35
ΔP_{Cexit} (bar)	2.5
Material	Flour
ρ_p (kg.m^{-3})	1530
D_{int} (mm)	20 - 36

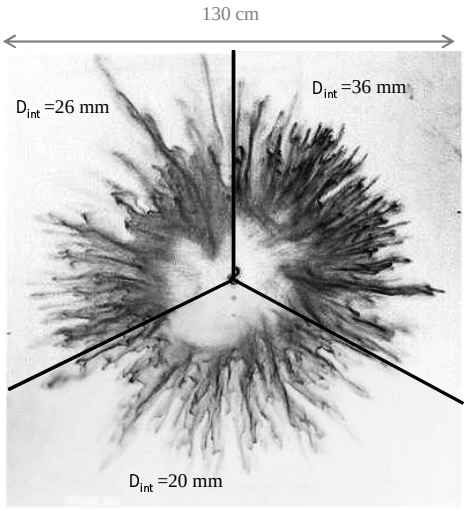

Fig. 11 Photographs showing the influence of internal particle ring diameter on the number of jets at t=40 ms. The variable conditions are given in the lower table.

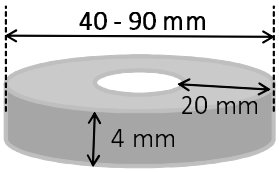

M_{sw}	1.35
ΔP_{Cexit} (bar)	2.5
Material	Flour
ρ_p (kg.m^{-3})	1530
D_{ext} (mm)	40 - 90

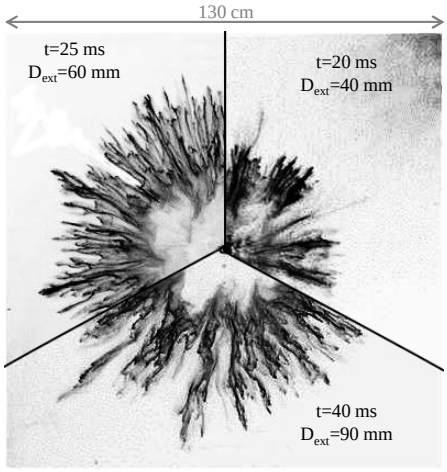

Fig. 12 Photographs showing the influence of external particle ring diameter on the number of jets. The thickness of the particle layer is kept constant. The range of external diameter variations is given in the bottom table.

3.6 Influence of friction on the Hele-Shaw plate on the particle dispersion

A possible mechanism for particle jets size selection is based on inter-granular friction. To assess the ability of frictional forces to influence the selected size, the influence of plate surface roughness on the particle motion is studied. Three surface roughnesses were tested: one smooth and two having different roughnesses. The roughness surfaces were obtained by sticking sheets of sandpaper

on the plate. In Fig.13, results from experiment conducted with two different surface roughnesses are shown. A half smooth, on the right, and a half rough, on the left. In this photo, it is possible to observe the difference on the selection of the jet number. It appears that the number of jets is not the same in these two parts. In addition, the graph in Fig.14 shows several experimental points plotted for a smooth surface and for two different rough surfaces. It represents the number of jets N_j versus the initial overpressure $\Delta P_{C_{exit}}$. The surfaces roughnesses are given in the figure. It appears that the selection of the jet number is clearly different between a smooth surface and a rough one corresponding to larger friction. The number of jets for the rough state is almost twice. However, there is no difference between the two rough states used in this study. Although three-dimensional effects are present in the Hele-Shaw cell (this is a quasi two-dimensional apparatus), the addition of sand paper in the bottom plate induces a modification in the expansion velocity of particles, for the same conditions, and so it is clear that the friction (induced by the air or in our case by the plate surface) acts on the number of particle jets. Therefore it is reasonable to conclude that the number of jets increases with increasing friction.

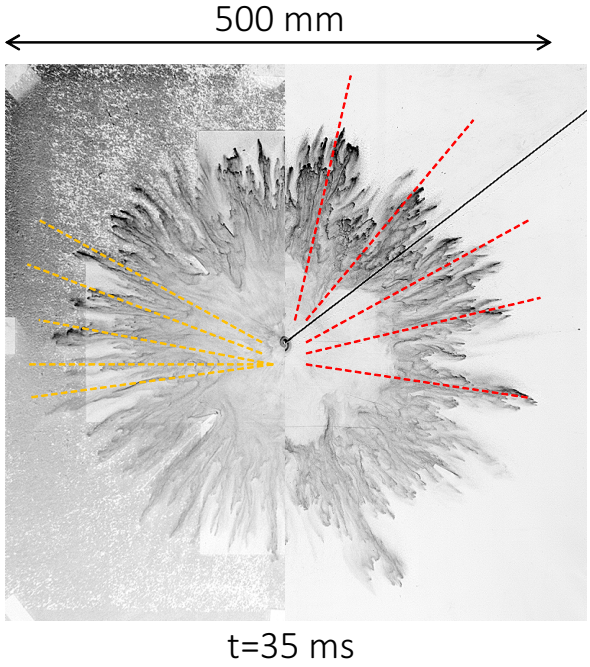

Fig. 13 Photographs showing the influence of wall friction at the Hele-Shaw surface during dispersion of two identical flour particle rings submitted to the same conditions. On the left, friction has been added on the bottom plate. On the right, the bottom plate stays smooth. The initial overpressure at the center of the rings is 2.5 bars.

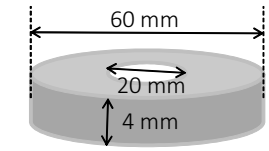

Material	Flour
ϕ_p (µm)	10
ρ_p (kg.m^{-3})	1530

Sandpaper type	Grain size (µm)
40	425
280	52,2

ΔP_{Cexit} (bar)	0.5 – 4.5

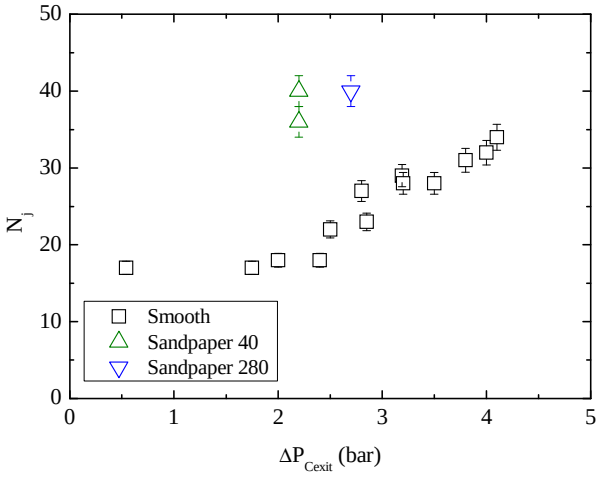

Fig. 14 Number of jets N_j versus the initial pressure jump $\Delta P_{C_{exit}}$ for different surface frictions at the Hele-Shaw cell plate. The variable conditions are given in the bottom table.

3.7 Particle jets: a fractal behaviour?

A preliminary study of the fractal dimension versus time is carried out. It is made for several rings of flour having different size as well as a ring of polystyrene with a particle diameter of 10 μm. Another variable parameter is the Mach number of the incident shock wave. In Fig.15, the fractal dimension D_f as a function of time is plotted for various incident shock waves. For this presentation, classical algorithm of "box-counting" via Matlab was used. Sizes of boxes are 32 square pixels for the first passage then 16 and 8 square pixels. The camera resolution is 1,024 square pixels. Thereby, the fractal dimension of the expanding ring evolves as the function of time, i.e. during dispersion. The evolution of the fractal dimension versus time ranges from 1.1 at baseline up to 1.4 as asymptotic value when time approaches "infinity". This tendency has already been mentioned in studies where the growth of the fractal dimension of an interface, after interaction between a shock wave and a rectangular block of SF_6, is measured [20,21]. In these articles, the fractal dimension also varies from 1.1 to 1.4. It is explained, in these papers, that the initial value of the fractal dimension (1.1) reflects the fact that the flow is laminar. This value increases with growth of instabilities and the final value is similar to a fully developed turbulent region. According to them, this increase in the fractal dimension is closely related to the mixing progress. It represents the transition to turbulence in the Richtmyer-Meshkov instability development. Further studies were made on the size analysis of fractal after explosions [22]. According to the definition of the fractal dimension, the shape of the pattern changes with time [20,21]. Several types of jets in the present study are

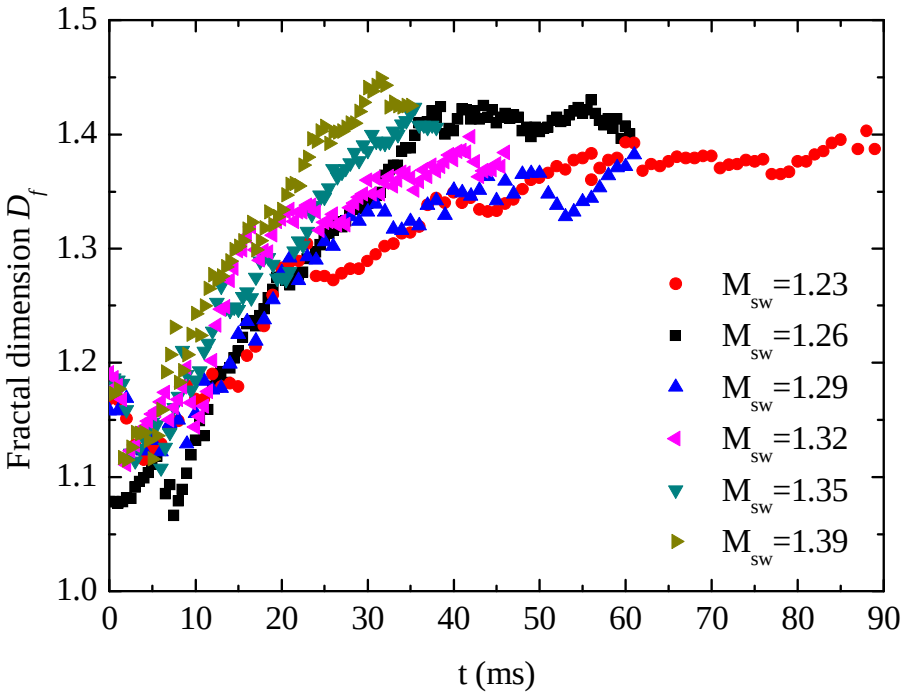

Fig. 15 Fractal dimension D_f versus time for different shock wave strengths. The geometry of the particle rings is the same for all investigated cases.

considered generating different fractal dimensions. In addition, the rise time of the curves shown in Fig.15 is variable. Indeed, it is faster when the Mach number of the incident shock wave is higher. Therefore, the dispersion of the particles and the formation of jets are faster. This reflects that the evolution of patterns is faster to its final value. Such method enables comparison of jets between specific experiments. Information on fractal dimension could also be useful as an additional criterion for comparison between experimental and numerical studies on the selection of number of jets. The curve corresponding to the evolution of the fractal dimension of a flour ring subjected to an incident shock wave of Mach number of 1.23 is plotted in Fig.16. The equation of the fitted curve is:

– $D_f = 1.37(1 - e^{-\frac{(t+17)}{13}})$

This equation follows the one $D_f = k(1 - e^{-\frac{t'}{\tau}})$ where t'=t+17 and k=1.37. The characteristic time is τ=13 ms. The usefulness of this characteristic time is to provide additional criterion for comparison between different experiments as well as comparison between experimental and numerical results.

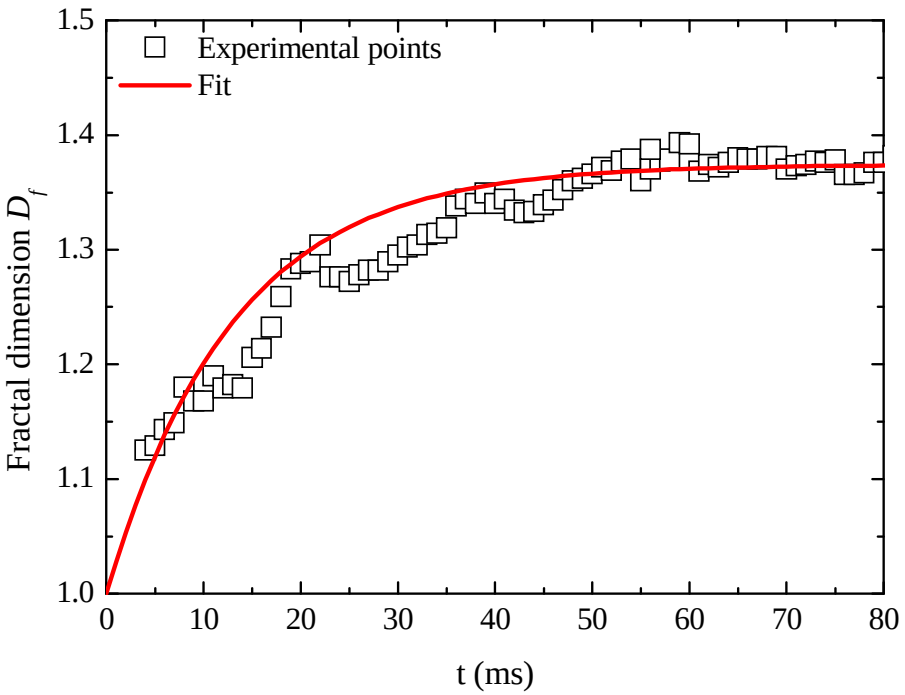

Fig. 16 Fractal dimension D_f versus time for a ring of 15 g of flour submitted to a 1.23 Mach number shock wave. The fitted curve has the following form: $D_f = 1.37(1-e^{-\frac{(t+17)}{13}})$.

3.8 Synthesis

Fig.17 provides a synthesis of the present experimental results. All points in this figure are taken from experiments done with different particle materials and different initial ring sizes (changes in the external diameter while keeping the thickness of the particle layer constant). Thus, the number of particle jets normalized by the ratio of the material density and by the initial perimeter of the external front is plotted versus the initial layer acceleration γ. It is easy to deduce from Fig. 17 that the number of jets is proportional to the initial perimeter of the external front. This means that the wavelength of the jet distribution is unchanged when the initial diameter of the particle ring changes, for a given initial impulse. Another empirical relationship that can be deduced from this figure is $N_j \mathrm{R}/\pi D_{ext}$=128.5+0.14$\gamma^{2.6}$. This relation describes the evolution of the particle jet number versus the initial layer acceleration and the influence of the material density of the ring. The material density used is taken into account by the factor R and the initial size of the ring is taken into account by the initial ring perimeter πD_{ext} where D_{ext} is the initial diameter of the particle ring. Results shown in Fig. 17 are valid for an initial particle layer acceleration up to 13 $m.s^{-2}$. Beyond this value, it seems to be a point of inflection (see the dashed line). From that value (13 $m.s^{-2}$) the number of jets

will not increase significantly and tends, as expected, to a maximum number of jets.

ϕ_p (µm)	10
γ (m.s^{-2})	0.8 - 17
Material	Flour Polystyrene PMMA Talc
ρ_p	1050 – 2700
D_{ext} (mm)	40 – 90

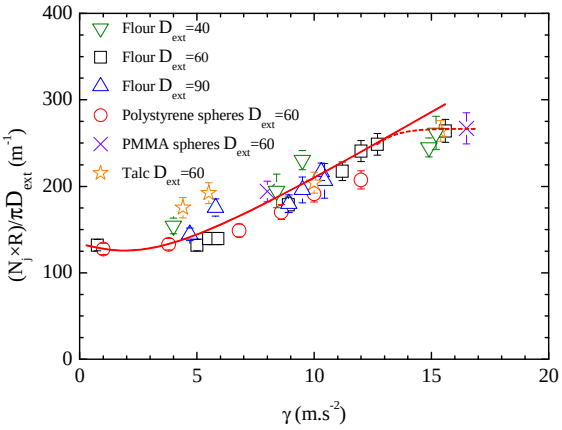

Fig. 17 Synthesis of all conditions used. The number of jets N_j, normalized by the density ratio R and the initial external perimeter of the particle ring πD_{ext}, is plotted versus the initial particle layer acceleration γ. The variable conditions are presented in the bottom table. The empirical correlation is the following: $N_j \mathrm{R}/\pi D_{ext}$=128.5+0.14$\gamma^{2.6}$.

4 Conclusion

The basic features of particle dispersion by weak blast wave has been described in earlier works. The present paper reports additional experiments carried out to determine the effect of variable ring geometry and other parameters on the number of particle jets formed. The experimental results are analysed and empirical relationships are obtained. The facility enables to observe the origin of the jets inside the dispersed particle cluster. We find that the particle jets are formed very early after the ring interaction with blast or shock waves. Then, the jet structures cross the particle layer, grows further-on toward the outer surface. Several particle materials and initial parameters have been tested. The influence of the pressure loading imposed to the particle ring, the particle diameter and density, the strength of the initial pressure pulse and the initial geometry of the ring have been studied for weak blast waves. Moreover, external conditions effecting the ring have been modified by changing the surface roughness of the Hele-Shaw cell plates in the way to detect the evolution of the particle jets. Empirical relationships extracted from the results allow to quantify the number of jets as a function of the overpressure imposed initially into the center of the ring, the initial size of the ring, the density of the material used and consequently the initial acceleration of the particle front. An empirical relationship is proposed: $N_j = (128.5 + 0.14\gamma^{2.6})\pi D_{ext}/R$, where N_j is the particle jet number, γ the initial acceleration of the particle front, D_{ext}

the initial diameter of the ring and R the ratio between the density of the particles and the density of the material (polystyrene spheres in the present study).

Acknowledgements CEA Gramat is gratefully acknowledged by the authors.

References

1. G. Ben-Dor, O. Igra and T. Elperin: Handbook of shock waves **vol 2** (2001).
2. V. Kedrinskiy, "Hydrodynamic aspects of explosive eruptions of volcanoes: simulation problems", Shock Waves **18**, 451-464 (2009).
3. D. Lohse, R. Bergmann, R. Mikkelsen, C. Zeilstra, D. van der Meer, M. Versluis, K. van der Weele, M. van der Hoef and H. Kuipers, "Impact on soft sand: void collapse and jet formation", Phys. Rev. lett. **93**, 198003 (2004).
4. D.L. Frost, S. Goroshin and F. Zhang, "Jet formation during explosive particle dispersal" *in Proceedings of the 21st Military Aspects of Blast and Shock*, Jerusalem, Israel (2010).
5. F. Zhang, D.L. Frost, P.A. Thibault and S.B. Murray, "Explosive dispersal of solid particles", Shock Waves, **10**, 431-443 (2001).
6. D.L. Frost, C. Ornthanalai, Z. Zarei, V. Tanguay and F. Zhang, "Particle momentum effects from the detonation of heterogeneous explosives", Journal of applied physics , **101**, 113529 1-14 (2007).
7. A.M. Milne, C. Parrish and I. Worland, "Dynamic fragmentation of blast mitigants", Shock Waves, **20**, 41-51 (2010).
8. C. Parrish and I. Worland, "Dynamic jet formation from mitigation materials",*in Proceedings of the 28th International Symposium on Shock Waves*, CD-Rom, Manchester, UK (2011).
9. D.L. Frost, Y. Grégoire, O. Petel, S. Goroshin and F. Zhang, "Particle jet formation during explosive dispersal os solid particles", Physics of fluids **24**, 091109 1-2 (2012)
10. D.L. Frost, J.F. Ruel, Z. Zarei, S. Goroshin, Y. Grégoire, F. Zhang, A.M. Milne, and A. Longbottom, "Explosive formation of coherent particle jets", *in Proceedings of the 22nd Military Aspects of Blast and Shock*, Bourges, 2012.
11. F. Zhang, R.C. Ripley, A. Yoshinaka, C. R. Findlay, J. Anderson, B. Von Rosen, "Explosive dispersal of solid particles", Shock Waves, **25**, 239-254 (2015).
12. V. Rodriguez, R. Saurel, G. Jourdan and L. Houas, "Solid-particle jet formation under shock-wave acceleration", Physical Review E **88**, 063011 (2013)
13. V. Rodriguez, R. Saurel, G. Jourdan and L. Houas, "External front instabilities induced by a shocked particle ring", Physical Review E **90**, 043013 (2014)
14. T. Xu, F.S. Lien, H. Ji and F. Zhang, "Formation of particle jetting in a cylindrical shock tube", Shock Waves **23**, 16 (2013)
15. Emmanuel Lapébie, CEA-Gramat, France, private communication
16. B. Sullivan, W.E. Engebretson and M.L. Anderson, "The relation of particle size to certain flour characterization", Cereal Chemistry **37**, 436-455 (1960)
17. R.R. Irani, and W.S. Fong, "Measurements of the particle size distribution of flour", Cereal Chemistry **38**, 67-75 (1961)
18. J. Ferrer, J.F. Montes, M.A. Vilarino, R.W. Light and R. Garcia-Valero, "Influence of particle size on extrapleural talc dissemination after talc slurry pleurodesis", CHEST **122**, 1018-1027 (2002)
19. R.C. Ripley, L. Donahue and F. Zhang, "Jetting instabilities of particles from explosive dispersal", AIP Conf. Proc. **1426**, 1615-1618 (2012).
20. H.D. Ng, H.A. Abderrahmane, K.R. Bates and N. Nikiforakis, "The growth of fractal dimension of an interface evolution from the interaction of a shock wave with a rectangular block of SF_6", Nonlinear Science and Numerical Simulation **16**, 4158-4162 (2011).
21. P. Vorobieff, P.M. Rightley, and R.F. Benjamin, "Shock-driven gas curtain: fractal dimension evolution in transition to turbulence", Physica D **133**, 469-476 (1999).
22. Y. Dong, H. Li and L. Yi, "Study of FAE explosive image analysis based on the fractal dimension", Journal of Mathematics Research **1**, 102-107 (2009).